JGR

RESEARCH ARTICLE

Key Points:
- Lightning in TCs over NP is more likely to occur in TD and TS intensity level
- Lightning in the inner core may be a better indicator for NP RI prediction
- A different pattern of lightning and TC intensity change exists among basins

Correspondence to:
W. Zhang,
zhangwj@cams.cma.gov.cn

Relationship between lightning activity and tropical cyclone intensity over the northwest Pacific

Wenjuan Zhang[1,2], Yijun Zhang[1,2], Dong Zheng[1,2], Fei Wang[1,2], and Liangtao Xu[1,2,3]

[1]State Key Laboratory of Severe Weather, Chinese Academy of Meteorological Sciences, Beijing, China, [2]Laboratory of Lightning Physics and Protection Engineering, Chinese Academy of Meteorological Sciences, Beijing, China, [3]College of Earth Science, University of Chinese Academy of Sciences, Beijing, China

Abstract Lightning data from the World Wide Lightning Location Network along with tropical cyclone (TC) track and intensity data from the China Meteorological Administration are used to study lightning activity in TCs over the northwest Pacific from 2005 to 2009 and to investigate the relationship between inner core lightning and TC intensity changes. Lightning in TCs over the northwest Pacific is more likely to occur in weak storms at tropical depression ($10.8–17.1\,\mathrm{m\,s^{-1}}$) and tropical storm ($17.2–24.4\,\mathrm{m\,s^{-1}}$) intensity levels, in agreement with past studies of Atlantic hurricanes. The greatest lightning density (LD) in the inner core appears in storms undergoing an intensity change of $15–25\,\mathrm{m\,s^{-1}}$ during the next 24 h. Lightning is observed in all storm intensity change categories: rapid intensification (RI), average intensity change (AIC), and rapid weakening (RW). The differences in LD between RI and RW are largest in the inner core, and the LD for RI cases is larger than for RW cases in the inner core (0–100 km). Lightning activity there, rather than in the outer rainbands, may be a better indicator for RI prediction in northwest Pacific storms. There was a marked increase in the lightning density of inner core during the RI stage for Super Typhoon Rammasun (2008). Satellite data for this storm show that the RI stage had the highest cloud top height and coldest cloud top temperatures, with all the minimum black body temperature values being below 200 K in the inner core.

1. Introduction

There has been significant development in the prediction of tropical cyclone (TC) tracks over the past few decades due to advances in detection technology and a deeper understanding of physical and dynamical processes, whereas the accuracy of intensity forecasts has not improved as rapidly [*Marks and Shay*, 1998; *Shen et al.*, 2006; *DeMaria et al.*, 2014]. Physical processes leading to TC intensification rely not only on large-scale dynamics but also on small-scale convective bursts within the inner core. Most of the current platforms do not provide continuous observation (e.g., low sample rate of satellite orbits, spatiotemporal restriction of radar, and aircraft) of convective bursts, limiting the prediction of TC bursts and rapid intensification (RI) [*Fierro et al.*, 2011]. Lightning activity is closely related to the dynamical and microphysical processes of thunderstorms and can be used to study the evolution of convective structure [*Rust et al.*, 1981; *Rutledge et al.*, 1993; *MacGorman and Morgenstern*, 1998]. Additionally, lightning data can provide more precise locations of strong updrafts than radars and infrared satellites [*Molinari et al.*, 1999]. Thus, a combination of large-scale ground-based lightning networks such as the World Wide Lightning Location Network (WWLLN) [*Rodger et al.*, 2005] and the Global Lightning Dataset (GLD360) [*Demetriades et al.*, 2010], with current platforms such as aircraft (both in situ and radar observations), and geostationary and low-Earth-orbiting satellites, could overcome the spatiotemporal limitations of current platforms and provide continuous observation throughout the TC lifetime.

Lightning activity within the inner core (within 100 km or so) and eyewall region of TCs has been investigated in previous studies. Lightning in the inner core is usually sparse; however, significant electrical activity can occur in this region according to a survey of 46 flight reports dating from 1980 by *Black and Hallett* [1999]. Eyewall lightning outbreaks that occur prior to or during most major intensity changes of storms [*Solorzano et al.*, 2008] and lightning bursts in the eyewall of mature TCs are believed to be good indicators of imminent intensification of these systems [*Lyons and Keen*, 1994; *Fierro et al.*, 2007; *Pan et al.*, 2010]. *Molinari et al.* [1994] found eyewall lightning outbreaks prior to and during periods of intensification of Hurricane Andrew (1992) using the National Lightning Detection Network (NLDN). They found that flashes in the eyewall occurred mainly when clouds were deepening dramatically, because at such times

the eyewall convection was growing rapidly and updrafts would be more likely to contain liquid water in the mixed-phase region. *Black and Hallett* [1999] observed many lightning discharges when storms were in the RI phase. Similar findings have also been reported for Hurricanes Katrina and Rita (2005) using the Long-Range Lightning Detection Network (LLDN) and the Tropical Rainfall Measuring Mission (TRMM) satellite [*Squires and Businger*, 2008]. *Molinari et al.* [1999] examined nine Atlantic basin hurricanes and proposed a relationship between inner core lightning and TC intensity change: lightning outbreak in the core of a weakening, steady, or slowly deepening hurricane might indicate it was about to rapidly intensify. Narrow bipolar events (NBEs) provide unique height information for lightning activity in the eyewall and may be used to track intense convective bursts within hurricanes. *Abarca et al.* [2011] found that intensifying Atlantic basin TCs had an average of 1.5 to 2 times more flashes in the inner core than nonintensifying cases. Analysis of intracloud NBEs using the Los Alamos Sferic Array for Hurricanes Rita and Katrina (2005) by *Fierro et al.* [2011] revealed an increase in discharge heights within the eyewall during the period of deepening, followed by a rapid decrease in the discharge height of intracloud lightning. The above studies reveal a possible relationship between inner core lightning and TC intensification, and suggest that the change of lightning activity in the inner core, particularly lightning outbreak in the inner core, may indicate the enhancement of TC intensity.

In addition to lightning frequency and density, the polarity of lightning in the inner core can also provide useful information about TC intensity change. Positive eyewall lightning tended to occur directly under the highest cloud tops and occurred radially outside of the negative flashes in Hurricane Andrew (1992) [*Molinari et al.*, 1994]. This reveals an outward tilt of the eyewall with height, and the updraft in the eyewall shifts the region of positive flash slightly outward from the region of negative flash. *Thomas et al.* [2010] reported that the number of positive cloud-to-ground lightning flashes in the inner core increased prior to and during periods of rapid weakening (RW) in Hurricanes Emily, Katrina, and Rita (2005). This suggests that real-time polarity observations of TC lightning might provide a useful tool for forecasting intensity change.

The hurricane inner core appears to resemble deep, weakly electrified oceanic monsoonal convection [*Molinari et al.*, 1994]. Nevertheless, it represents a unique atmospheric phenomenon with its own dynamical, microphysical, and electrical organization [*Molinari et al.*, 1999]. Lightning activity in the inner core is relatively weak in general because of the absence of supercooled water and lack of strong updrafts [*Black and Hallett*, 1986; *Black et al.*, 1996]. Large flash density in the inner core occurs only when strong convection develops, particularly in intensifying weak storms [*Abarca et al.*, 2011]. *Black and Hallett* [1999] related electrical activity in the inner core to the microphysical cloud structure and attributed lightning occurrence to strong vertical velocity and the presence of supercooled liquid cloud droplets extending to temperatures below $-20°C$. In agreement with *Black and Hallett* [1999], *Reinhart et al.* [2014] identified three common characteristics of hurricane electrified regions: (1) strong updrafts of $10–20\,m\,s^{-1}$, (2) deep mixed-phase layers, and (3) microphysical environments consisting of graupel, small ice particles, and supercooled water.

When storms experience RI, the mixed-phase region extends to much higher altitudes than normal, and vertical wind speeds of $>20\,m\,s^{-1}$ are observed [*Black and Hallett*, 1999]. Aircraft flight observations show that vertical motion in the eyewall is enhanced when the storm undergoes RI, following a minimum of the eye diameter and attainment of the steepest vertical slope of the eyewall structure [*Squires and Businger*, 2008]. The stronger vertical convection results in more effective electrification, leading to higher lightning flash density and outbreaks of lightning in the eyewall. As the storm develops, preexisting ice in the inner core efficiently nucleates supercooled water and the charging mechanism may become less effective, resulting in weak lightning activity after the outbreak of eyewall lightning [*Abarca et al.*, 2011].

Modeling results based on quantifying the flow of energy from asymmetric heat sources to the kinetic energy of the wind field of a symmetric vortex [*Nolan et al.*, 2007] have indicated that rapid heat release in the tall convective towers [*Kelley et al.*, 2004] can lead to RI. The occurrence of such a small-scale, strong convective tower in the interior of the TC is caused by a sudden increase of outflow at higher altitudes and indicates its thermally asymmetric structure. When one or more extremely tall convective towers exist in the eyewall, the chance of TC intensification increases [*Kelley et al.*, 2005]. Since lightning activity is significantly associated with the microphysics and dynamics of this small-scale convection, there is potential for using lightning data to provide some in situ information and to help improve forecasts of TC

intensification. Therefore, lightning combined with other observational data can contribute to a more comprehensive understanding of the structure of the internal convection and TC intensity change.

In this work, we use lightning data from the WWLLN, along with storm track and intensity data from the China Meteorological Administration, to study the characteristics of lightning activity in TCs over the northwest Pacific and to investigate its relationship to TC intensity changes. In section 2, the data sources and methods for the study are described. In section 3, the relationship between lightning and TC intensity and the results of a case study are presented. Lightning patterns in the Pacific basin and the implications of using inner core lightning to examine rapid changes in TC intensity are discussed in section 4. Finally, the main conclusions of this study are given in section 5.

2. Data and Methods

2.1. Lightning Data

Lightning data from January 2005 to December 2009 of the WWLLN are analyzed in this study. The WWLLN was established in 2004 [*Rodger et al.*, 2006] and is operated by the University of Washington. With 68 sensors as of October 2012 [*Virts et al.*, 2013], the network determines lightning locations around the globe in real time. It uses very low frequency (3–30 kHz) radio wave receivers to identify the time of group arrival (TOGA) from a lightning stroke. The TOGA is determined relative to GPS at each site and sent to a central processor that combines the TOGAs from at least five sensors to determine the source lightning location and calculate information about the time, latitude, and longitude of the lightning [*Rodger et al.*, 2004]. The stable propagation and low attenuation of very low frequency waves allows a wide spacing of sensors of several thousand kilometers so that global lightning location can be provided by the WWLLN [*Dowden et al.*, 2002].

The increasing number of WWLLN stations and a new algorithm implemented in 2005 have led to an improvement of 63% in detection efficiency (DE) [*Rodger et al.*, 2008]. The location accuracy and DE of the WWLLN have been examined by comparison with regional lightning detection networks in Brazil [*Lay et al.*, 2004], Australia [*Rodger et al.*, 2004, 2005], the United States [*Jacobson et al.*, 2006; *Abarca et al.*, 2010], New Zealand [*Rodger et al.*, 2006], and Canada [*Abreu et al.*, 2010] (Table 1). These studies indicate that WWLLN detects both cloud-to-ground lightning strokes and some large intracloud pulses, and is most sensitive to high peak current lightning strokes [*Rodger et al.*, 2006, 2008; *Hutchins et al.*, 2012]. Studies have also been conducted to compare the network with satellite measurements. Using data from the Lightning Imaging Sensor/Optical Transient Detector (LIS/OTD), *Pan et al.* [2013] found that the diurnal variations of lightning over land in the WWLLN and LIS/OTD data sets showed similar patterns, but lightning density (LD) detected by the WWLLN was in general 1 order of magnitude lower than that from the LIS/OTD. *Virts et al.* [2013] also found that the WWLLN lightning climatology appeared to be consistent with the LIS climatology, but the sample sizes of WWLLN were 2 orders of magnitude larger than is feasible with the LIS.

The WWLLN can be successfully used to study the temporal and spatial structure of lightning activity in TCs when storms are far away from regional ground-based lightning networks. Although WWLLN has been in operation for only a few years and the DE is fairly low, the correlations between TC lightning detected by WWLLN with the NLDN and LLDN are shown to be high [*Abarca et al.*, 2011], and more stations are continually being added to the network. The network can monitor lightning over the entire globe, offering the possibility of using the data in the study of TCs over deep oceans, and particularly to help distinguish between intensifying and nonintensifying TCs [*DeMaria and DeMaria*, 2009; *Price et al.*, 2009; *Thomas et al.*, 2010]. As WWLLN DE has varied considerably over the period of this study [*Rodger et al.*, 2008], a method of data calibration is needed. *Hutchins et al.* [2012] demonstrated a technique that uses the energy data collected by WWLLN to estimate the relative DE over the Earth and developed a model for DE correction of global LD. On the other hand, *DeMaria et al.* [2012] and *Bovalo et al.* [2014] used the long-term global LD climatology estimated from TRMM LIS/OTD [*Boccippio et al.*, 2002] to adjust their results from WWLLN in the Atlantic, East Pacific, and Southwest Indian Ocean. The WWLLN data were multiplied by adjustment factors that make the annual average LD equal to that from the LIS/OTD climatology. In the present study, WWLLN data are calibrated following the procedures used by *DeMaria et al.* [2012] and *Bovalo et al.* [2014]. The mean annual flash rate climatology data [*Cecil et al.*, 2014], with units of flashes $km^{-2} yr^{-1}$, on a 0.5°

Table 1. Comparison Studies of WWLLN Data With Regional Lightning Networks

Study	Regional Network/Country	Sites[a]	Time Period	DE (Number of Shared Strokes/Regional Network Strokes)[b]	DE for High Peak Current	Mean LA[d] (km)
Lay et al. [2004]	BIN/Brazil	11	6, 7, 14, 20, and 21 Mar 2003	Total = 0.5% (289/63,893)	NA[c]	20.25 ± 13.5, Lat = 3.2, Lon = 7.3
Rodger et al. [2004]	Kattron/Australia	11	23–24 Jan 2002	Total = 1.4% (426/30,402)	NA	30
Rodger et al. [2005]	Kattron/Australia	18	13 Jan 2004	Total = 24.8% (5,006/20,182)	NA	3.4
Jacobson et al. [2006]	LASA/United States	19	27 Apr to 30 Sep 2004	Total = 0.8% (71,362/8,923,316), CG = 1.3% (52,728/4,196,004), IC = 0.5% (21,437/4,727,312)	$|I_p|$ > 30 kA, ~4%	15–20
Rodger et al. [2006]	NZLDN/New Zealand	20	1 Oct 2003 to 31 Dec 2004	Total = 2.7% (6,113/224,221), CG = 2.9% (5,923/204,411), IC = 1.0% (190/19,810)	$|I_p|$ > 50 kA, ~10%	NA
Abreu et al. [2010]	CLDN/Canada	29	1 May to 31 Aug 2008	Total = 2.8% (19,128/677,406)	$|I_p|$ > 20 kA, 11.3%; $|I_p|$ > 120 kA, 75.8%	7.24 ± 6.34, Lat = −3.14 ± 5.91, Lon = 1.62 ± 6.71
Abarca et al. [2010]	NLDN/United States	38	5 Apr 2006 to 31 Mar 2009	DE 6.2% (6,154,394/99,359,988), CG 10.3% (2,558,809/24,839,997), IC 4.8% (3,595,585/74,519,991)	$|I_p|$ > 35kA 10%	Lat = 4.03, Lon = 4.98

[a] The number of WWLLN sites when studied.
[b] Total, CG, and IC indicate the detection efficiency for total, cloud-to-ground, and intracloud strokes, respectively.
[c] NA indicates that no data are available.
[d] Lat and Lon mean latitudinal and longitudinal offset in location errors.

Table 2. Adjustment Factors for WWLLN LD Based On the LIS/OTD Climatology in the Northwest Pacific and Comparisons With Other Ocean Basins

Year	Northwest Pacific 0°–45°N, 100°–170°E		Atlantic[a] 0°–50°N, 100°–10°W		East Pacific[a] 0°–40°N, 180°–100°W		South West Indian Ocean[b] 50°S to 10°N, 30°–110°E		Northwest Pacific[c] 0°–45°N, 135°–180°E	
	Adjustment Factor	DE (%)	Adjustment Factor	DE (%)	Adjustment Factor	DE (%)	Adjustment Factor	DE (%)	Adjustment Factor	DE (%)
2005	16.3	6.1	37.5	2.7	110.1	0.9	50.0	2.0	11.27	8.9
2006	12.0	8.3	24.1	4.1	31.1	3.2	29.4	3.4	11	9.1
2007	13.3	7.5	22.8	4.4	30.2	3.3	20.0	5.0	12.46	8.0
2008	9.9	10.1	16.7	6.0	15.2	6.6	21.3	4.7	5.32	18.8
2009	7.4	13.5	6.8	14.7	5.0	20.0	15.2	6.6	3.01	33.2

[a]Adjustment factors by *DeMaria et al*. [2012].
[b]Adjustment factors by *Bovalo et al*. [2012, 2014].
[c]Adjustment factors by *Pan et al*. [2014].

latitude-longitude grid from the LIS/OTD are used as ground truth. The ratios between the mean annual lightning climatology from the LIS/OTD and the annual average LD from the WWLLN over the northwest Pacific domain (0°–45°N, 100°–110°E) are calculated as adjustment factors. Thus, for each year of the study, LDs measured from the WWLLN are multiplied by the adjustment factor for that year to give the total lightning.

Table 2 lists the adjustment factors for WWLLN annual LD over the northwest Pacific and comparisons with the Atlantic, East Pacific, and the South West Indian Ocean. There is an increase in WWLLN DE (inverse of the adjustment factors) for all four basins. However, two features of DE over the northwest Pacific are evident compared with other basins. First, the average DE for each year of the study over the northwest Pacific is larger than that for the other three basins, especially in 2005. The average DE over the northwest Pacific in 2005 is 6.1% (in this study) and 8.9% [*Pan et al*., 2014], while it is only 1%–3% for the Atlantic, East Pacific, and the South West Indian Ocean (Table 2). Second, the growth in DE for the northwest Pacific over the years is steady and not as significant as for the Atlantic and East Pacific basins. In the northwest Pacific, DE increases from 6.1% in 2005 to 13.5% in 2009 in this study, and from 8.9% in 2005 to 33.2% in 2009 in the study of *Pan et al*. [2014]. The rate of increase is similar to the results of *Bovalo et al*. [2012], who found a small increase in DE in the South West Indian Ocean, from 2.0% in 2005 to 6.6% in 2009. However, for the Atlantic and East Pacific, *DeMaria et al*. [2012] found values of DE ranging from 2.7% and 0.9% in 2005 to 14.7% and 20.2% in 2009, showing a much larger rate of increase.

The relatively high DE over the northwest Pacific and the differences in the rate of increase between the northwest Pacific and other basins are believed to be due to the global coverage and increase in station numbers in the WWLLN. In the very early years (2004–2005) of the WWLLN, the network did not provide equal coverage of all regions of the Earth. Many stations were clustered in Asia and Australia (see Figure 1 of *Rodger et al*. [2004] and Figure 1 of *Rodger et al*. [2005]), so WWLLN measured a much higher percentage of lightning discharges in the Western Pacific at that time. *Rodger et al*. [2006] described the April 2006 WWLLN data with a first principles DE model and found that the WWLLN had the highest DE in the western Pacific region, with DE of ~10%. In the following years, the network expanded from a limited number of stations to 38 stations by 2009 that covered much of the globe. The additional stations were located mainly in northern Europe, eastern South America, and the South Atlantic, and have led to a major improvement in DE in these regions.

2.2. Tropical Cyclone Data

There were 116 TCs from 2005 to 2009 in the northwest Pacific. The data on TC track and intensity are obtained from the China Meteorological Administration best-track data set, which gives data at 6-hourly intervals for the center latitude and longitude, the maximum sustained surface wind speed, and the minimum central pressure of the storms. Hourly center position and intensity are obtained by spline interpolation to estimate the position of lightning flashes relative to the storm center. Storm data are restricted to the following two conditions: (i) the location of the storm center was over water, and (ii) the intensity of the storm reached tropical depression strength, i.e., maximum sustained surface wind speed of $> 10.8 \, \mathrm{m \, s^{-1}}$.

According to the national standard for TC levels proposed by the China Meteorological Administration, TC intensities are classified into six levels depending on the mean maximum wind speed: tropical depression (TD; 10.8–17.1 m s^{-1}), tropical storm (TS; 17.2–24.4 m s^{-1}), severe tropical storm (STS; 24.5–32.6 m s^{-1}), typhoon (TY; 32.7–41.4 m s^{-1}), severe typhoon (STY; 41.5–50.9 m s^{-1}), and super typhoon (SuperTY; ≥51.0 m s^{-1}). The 116 TCs between 2005 and 2009 over the northwest Pacific examined in this study include 28 TSs, 21 STSs, 34 TYs, 11 STYs, and 22 SuperTYs.

The National Centers for Environmental Prediction global final analysis data set at 1°resolution and 6-hourly intervals is used to compute environmental vertical wind shear. Vertical wind shear is calculated by averaging the 850 and 200 hPa 6 h horizontal wind vectors over a radius of 500 km from the TC center, and then computing the magnitude in difference.

2.3. Black Body Temperature Data

Black body temperature (TBB) data from the Multi-functional Transport Satellite (MTSAT-1R) are used as an indicator of cumulus clouds for Super Typhoon Rammasun (2008). MTSAT-1R is a geostationary satellite launched in February 2005 by the Japan Meteorological Agency (http://weather.is.kochi-u.ac.jp/archive-e. html), as the successor to GOES 9. It covers East Asia and the western Pacific region from a position about 140°E at an altitude of 35,800 km above the equator. Imagery from the satellite covers the region with latitudes from 70°N to 20°S and longitudes 70°E–160°E. MTSAT-1R provides imagery from four infrared sensors and one visible sensor. Hourly images from infrared channel 1 are used in this study, which is in the 10.3–11.3 μm spectral window and has a spatial resolution of 0.05° × 0.05°. In this wavelength range, the reduction in strength of electromagnetic waves by atmospheric absorption is small, and the observed TBB accurately represents the physical temperatures of objects. Therefore, TBB can properly detect the cloud top, and its use is appropriate for investigating cumulus activity [*Taniguchi and Koike*, 2008].

2.4. Data Sample

For analysis, data are grouped by 6 h period in accordance with the best track as in *Abarca et al.* [2011] and *DeMaria et al.* [2012], called individual time periods (ITPs). There are 2370 ITPs for the 116 TCs. Each ITP has time, center location, storm intensity, and future intensity at 6 h, 12 h, and 24 h intervals, as well as lightning distribution. Lightning in each ITP is defined as the discharges within 500 km of the hourly interpolated storm center. No minimum lightning flash criteria are used in this study. As long as one flash occurred in an ITP, it is included in the data sample.

A number of studies have described the radial distribution of TC lightning; however, the values of TC radius varied among the studies. For Atlantic TCs, radii of about 300 km were considered as boundaries of the outer rainband. *Samsury and Orville* [1994] chose radii of 250 km from the storm center to study lightning associated with precipitation in Hurricane Hugo (1989). *Molinari et al.* [1994, 1999] subdivided hurricanes into 20 km bins up to 300 km from the storm center and found three zones of distinct electrical characteristics. *Squires and Businger* [2008] divided LD data into 25 km annular rings and grouped the radial bins into three regions: the eyewall (0–50 km), the inner rainband (75–175 km), and the outer rainband (175–300 km). *Abarca et al.* [2011] defined two storm regions: the inner core (0–100 km) and the outer bands (100–300 km). *DeMaria et al.* [2012] considered the areas of 0–50, 0–100, and 200–300 km radius to be the eyewall, inner core, and rainband regions, respectively. As the northwest Pacific TCs are significantly larger than Atlantic TCs (e.g., twice as large in *Merrill* [1984]; 0.7° latitude larger in *Liu and Chan* [1999]), radii of 500–800 km from the TC center have usually been selected for the study of lightning in the northwest Pacific [*Pan et al.*, 2010; *Zhang et al.*, 2012, 2013]. *Pan et al.* [2014] found the radii of typhoons over the northwest Pacific Ocean from 2005 to 2009 varied from 600 to 1300 km, with 80% within 600 km according to the MTSAT-1R satellite images. Therefore, a radius of 600 km was selected to represent TC size. *Zhang et al.* [2012] used a radius of 500 km as the limit of the outer rainbands for northwest Pacific TCs. With 20 km annular rings, they distinguished between the eyewall (0–60 km), the inner rainbands (60–180 km), and the outer rainbands (180–500 km). Based on the electrical characteristics in preliminary results for the northwest Pacific TCs, in the present study, each storm is divided into three regions: inner core, within 100 km of the storm center; inner rainband, 100–200 km from the center; and outer rainband, 200–500 km from the center. The radial extents of the three regions are close to the results of *Jiang et al.* [2013], who found mean radii of 82, 162, and 502 km for the inner core, inner rainband, and outer rainband, respectively, from 11 years of TRMM TC overpasses.
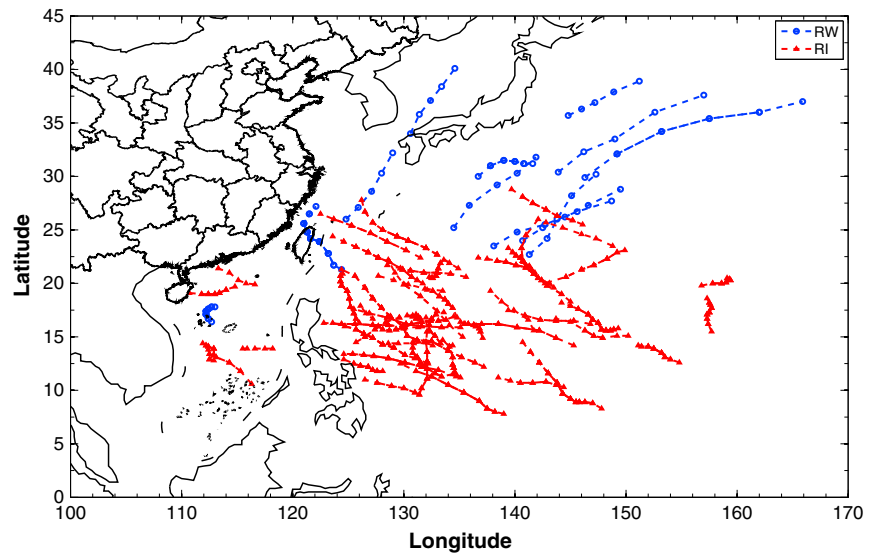
Figure 1. Six-hourly positions of RI cases in 44 TCs and RW cases in 11 TCs examined in this paper.

Lightning density is calculated in units of flashes per square kilometer per year ($fl\,km^{-2}\,yr^{-1}$). Hourly center positions are obtained from the best-track data by spline interpolation. Each lightning strike is then transformed to a storm-relative coordinate system and the range of each strike from the TC center is calculated. Each storm is divided into six rings from the storm center outward to 500 km (i.e., 0–50, 50–100, 200–200, 200–300, 300–400, and 400–500 km). When analyzing the radial distributions of LD, the LD is calculated by counting the number of strikes in each ITP for each ring and dividing by the area of that ring.

2.5. Definition of Categories of Intensity Change

Rapid intensification refers to a particular stage of TC development, and the definition of this stage is based on climate statistics. *Brand* [1973] first proposed a 24 h change in maximum sustained surface wind (ΔV_{max24}) of 50 kt (25.7 m s^{-1}) increase for a typhoon at sea as the criterion for RI over the northwest Pacific. *Kaplan and DeMaria* [2003] defined RI and RW as the 95th and 5th percentiles of ΔV_{max24} and found that a 24 h intensity increase of 30 kt (15.4 m s^{-1}) was close to the 95th percentile of the long-term Atlantic intensity change distribution for cyclones over water. An examination of the northwest Pacific intensity changes from 1970 to 2007 for cyclones over the northwest Pacific by *Shu et al.* [2012] showed that an increase in ΔV_{max24} of 15 m s^{-1} was close to the 95th percentile of the distribution and that a decrease of 20 m s^{-1} was close to the 5th percentile.

For consistency with *Shu et al.* [2012], an RI threshold of 15 m s^{-1} and an RW threshold of -20 m s^{-1} for ΔV_{max24} are employed in this study. Cases with ΔV_{max24} between -20 m s^{-1} and 15 m s^{-1} belong to the average intensity change (AIC) category. The data samples are thus separated into three intensity change categories: RI, AIC, and RW. The 116 TCs contribute a total of 170 RI ITP samples from 44 TCs, 20 RW ITP samples from 11 TCs, and 1969 AIC samples from 116 TCs. Figure 1 gives the 6-hourly positions of RI and RW ITP samples examined in this paper.

3. Results

A total of 1,179,152 lightning flashes were detected by the WWLLN for the 116 TCs over the northwest Pacific from 2005 to 2009. The percentages of lightning flashes in the inner core, inner rainbands, and outer rainbands are 11%, 14%, and 75%, respectively. The averaged LDs in these three regions are 130.4, 59.1, and 41.3 $fl\,km^{-2}\,yr^{-1}$ (a ratio of 3.1:1.4:1). The majority of lightning occurs in the outer rainbands, but the average LD in the inner core is the highest, consistent with the results of past studies [*DeMaria and DeMaria*, 2009; *Abarca et al.*, 2011; *DeMaria et al.*, 2012].
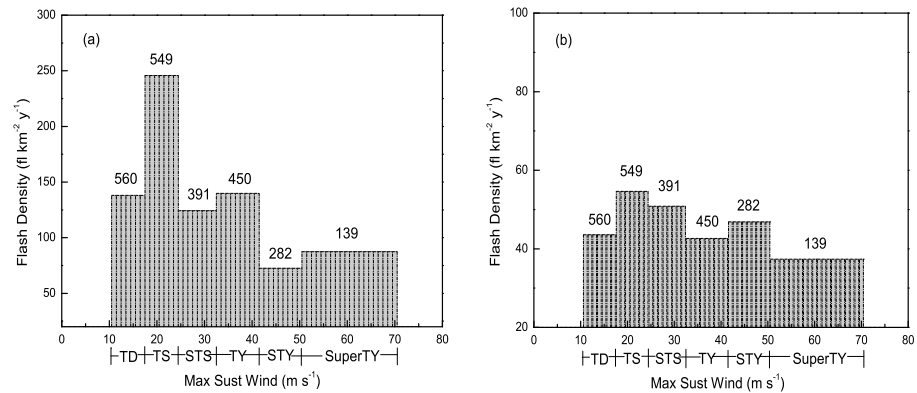
Figure 2. Lightning density as a function of storm intensity at the time the lightning occurred for (a) the inner core and (b) the outer rainbands. The number on each bar indicates the ITP samples used for the average.

3.1. Relationship Between Lightning and Tropical Cyclone Intensity

Figure 2 gives the average LD as a function of storm intensity at the time the lightning occurred for both the inner core and the outer rainbands. The changes of flash density with TC intensity show the same trend in the two regions, with an increase in weak storms (TD and TS) and then a decrease in storms stronger than STS. Figure 2 also shows that for all storm categories, the inner core has a much greater LD than the outer rainbands. Lightning occurs most often in TS intensity storms (17.2–$24.4 \, \mathrm{m \, s^{-1}}$ of maximum sustained wind) in the inner core, with LD of $245.8 \, \mathrm{fl \, km^{-2} \, yr^{-1}}$, and then less often in TY intensity storms. Lightning occurs least in STY intensity storms, with the LD reaching its minimum of $72.5 \, \mathrm{fl \, km^{-2} \, yr^{-1}}$ in the inner core. For the outer rainbands, lightning occurs most in TS intensity, as for the inner core, with LD of $54.6 \, \mathrm{fl \, km^{-2} \, yr^{-1}}$. The LD in the outer rainbands decreases when storms strengthen to intensity greater than TS. The minimum LD in the outer rainbands, $37.4 \, \mathrm{fl \, km^{-2} \, yr^{-1}}$, occurs when a storm is at SuperTY intensity.

The values of LD in the inner core and outer rainbands are much larger for weaker storms (TD and TS) than for severe typhoons and super typhoons, which is in agreement with the studies by *Cecil and Zipser* [1999], *Abarca et al.* [2011], and *DeMaria et al.* [2012]. *Molinari et al.* [1999] also found that the cloud-to-ground flash density maximum in the core was larger in marginal than in strong hurricanes. This is also true in the study of *Samsury and Orville* [1994], which showed that the cloud-to-ground flash density for Hurricane Jerry (1989) was more than an order of magnitude higher than for the more intense Hurricane Hugo (1989). Weak storms are often cyclones over warm water without a fully formed inner structure [*DeMaria et al.*, 2012]. Although not intensifying greatly, convection in the core in weak storms, particularly in intensifying weak storms, is usually more electrified and the charging mechanism is more efficient [*Molinari et al.*, 1999]. Once a stronger storm (hurricane or typhoon) develops, lightning in the inner core becomes episodic. The charging mechanism might be less effective for a larger content of preexisting ice particles in this region, and LD might be limited as the cyclone becomes organized [*Abarca et al.*, 2011].

The relationship between LD and TC intensity change is shown in Figure 3. Lightning occurs more often in cases undergoing small intensity changes ($|\Delta V_{\mathrm{max24}}| \leq 5 \, \mathrm{m \, s^{-1}}$) than for stronger intensity changes; the largest number of observed ITPs (1012) is for cases with small intensity changes. For both regions (Figures 3a and 3b), lightning occurs more often in storms strengthening ($\Delta V_{\mathrm{max24}} > 0 \, \mathrm{m \, s^{-1}}$) over the next 24 h than in weakening storms ($\Delta V_{\mathrm{max24}} < 0 \, \mathrm{m \, s^{-1}}$). The average LDs for strengthening and weakening storms are 450.8 and $123.3 \, \mathrm{fl \, km^{-2} \, yr^{-1}}$ in the inner core, and 111.9 and $62.9 \, \mathrm{fl \, km^{-2} \, yr^{-1}}$ in the outer rainbands, respectively, which shows that LD in strengthening storms is 2 to 4 times larger than in weakening storms. In both regions, the largest LD appears in storms undergoing intensity changes in the range $25 \, \mathrm{m \, s^{-1}} > \Delta V_{\mathrm{max24}} \geq 5 \, \mathrm{m \, s^{-1}}$ during the next 24 h. The lowest LD occurs at $\Delta V_{\mathrm{max24}} \leq -15 \, \mathrm{m \, s^{-1}}$ (i.e., RW) in the inner core (Figure 3a) and $\Delta V_{\mathrm{max24}} \geq 25 \, \mathrm{m \, s^{-1}}$ (i.e., RI) in the outer rainbands (Figure 3b), with LD in the inner core decreasing from 170.5 to $30.8 \, \mathrm{fl \, km^{-2} \, yr^{-1}}$ (Figure 3a) and from 45.2 to $21.3 \, \mathrm{fl \, km^{-2} \, yr^{-1}}$ (Figure 3b) in outer rainbands. The LDs decrease in both the inner core and outer rainbands when
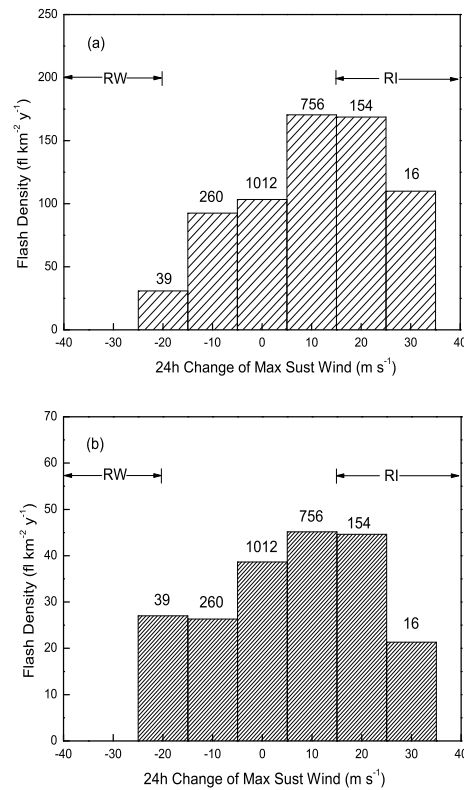
Figure 3. LD as a function of storm intensity change in the next 24 h for (a) the inner core and (b) the outer rainbands. The number on each bar indicates ITP samples used for the average.

storms undergo weakening during the next 24 h; however, lightning density shows a stronger relationship with TC intensity change in the inner core, where the variation of LD is more significant (Figure 3a). This result suggests that lightning activity in the inner core may be a better indicator than lightning activity in outer rainbands for predictions of TC intensity change in the northwest Pacific. This hypothesis will be examined in more detail in section 3.2.

3.2. Relationship Between Lightning and TC Rapid Intensity Change

Table 3 gives the distribution of samples including lightning in each intensity change category as a function of TC intensity level. The table shows that of the 2159 cases, AIC has the largest proportion of samples including lightning (91%) followed by the RI (8%) and then RW (1%) cases. This reveals that cyclones are generally in a relatively stable state when they are at sea and that rapid intensity changes (RI and RW) represent only a small proportion of intensity change cases. There are 170 RI cases and 20 RW cases, with obvious differences in their geographical distribution (Figure 1). RI generally occurs in the low-latitude area between 25°N and 5°N, mainly east of the Philippines. It is less likely to occur in middle to high latitudes north of 30°N. RW cases tend to occur farther north and east than the RI cases, and are distributed mainly in the high-latitude area from 20°N to 40°N, east of 125°E. There is no RI or RW in the low-latitude area between 0 and 5°N (Figure 1).

Table 3 also shows that lightning in RI cases is most likely to occur in TS category storms (55), followed by STS(48), TY (40), TD (15), and STY (12). This is consistent with *Kaplan et al.* [2010] and *Jiang* [2012], who found that tropical storms made up the highest percentages of RI cases in the Atlantic and eastern north Pacific basins. In contrast to RI, all RW cases are from TCs at typhoon and greater intensity, with the largest fraction from TY (13/20), then SuperTY (5/20), and STY (2/20). There are no RW cases including lightning from TD, TS, and STS storms. The average maximum surface wind speed for RW storms (43.8 m s^{-1}) is about a factor of 1.5–1.6 higher than that for AIC (28.4 m s^{-1}) and RI storms (27.2 m s^{-1}). The averaged ΔV_{max24} for RI and RW is 17.8 and -21.9 m s^{-1}, respectively (Table 3).

Figure 4 shows the LD as a function of radial distance from the TC center for RW, AIC, and RI cases. The most obvious feature is that LD for RI cases is larger than for RW cases in all radial bins, especially in the inner core region (0–100 km). Here LD is about 4.2 times greater for RI cases than for RW cases, and the difference in LD between RI and RW reaches its maximum. In RI cases, LD reaches a maximum at a radial distance of 0–50 km,

Table 3. Distribution of ITP Samples Containing Lightning in Each Intensity Change Category as a Function of Intensity Level[a]

| Category | Max Wind Speed Range (m s^{-1}) | Number of ITPs Containing Lightning in Intensity Levels | | | | | | | Number of TCs | Avg V_{max} (m s^{-1}) | Avg ΔV_{max24} (m s^{-1}) |
		TD	TS	STS	TY	STY	SuperTY	Total (%)			
RI	$\Delta V_{max24} \geq 15$	15	55	48	40	12	0	170 (8)	44	27.2	17.8
RW	$\Delta V_{max24} \leq -20$	0	0	0	13	2	5	20 (1)	11	43.8	-21.9
AIC	$-20 < \Delta V_{max24} < 15$	512	421	310	364	249	113	1969 (91)	116	28.4	1.2
Total (%)		527 (24)	476 (22)	358 (17)	417 (19)	263 (12)	118 (5)	2159 (100)			

[a]Also shown are the number of TCs, the average maximum surface wind speed (V_{max}), and the average wind speed change within the next 24 h (ΔV_{max24}) for different intensity change categories.
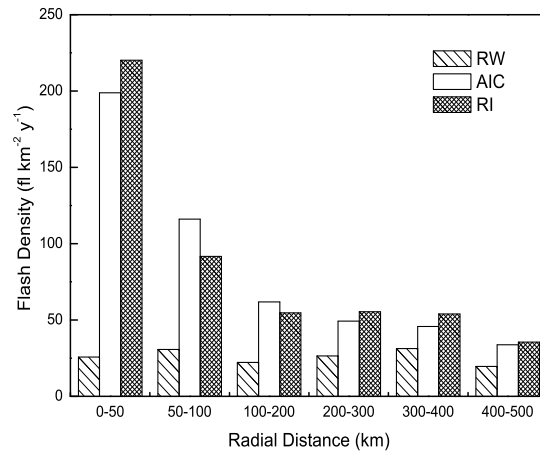
Figure 4. LD for RW, AIC, and RI cases as a function of radial distance from the TC center.

defined as the *eyewall region* in previous studies [e.g., *Molinari et al.*, 1994, 1999; *Squires and Businger*, 2008; *DeMaria et al.*, 2012; *Zhang et al.*, 2012, 2013], and the average LD in this region is about 8.7 times greater for RI cases (220.2 fl km^{-2} yr^{-1}) than for RW cases (25.8 fl km^{-2} yr^{-1}). Figure 4 shows that differences of LD among RW, AIC, and RI cases are not as significant in the outer rainbands (200–500 km), with LD of 25.1, 41.5, and 46.4 fl km^{-2} yr^{-1}, respectively. Thus, this result suggests that lightning activity in the inner core, rather than the outer rainbands, has predictive information for the RI of the storms, and that an increase of LD in the eyewall region may indicate a rapid strengthening in TC intensity.

Figure 5 shows the average LDs of the inner core, outer rainband, and the whole TC region as a function of the time between lightning occurring and the intensity change for the RI, RW, and AIC cases. The largest LD in the inner core occurs in RI cases, followed by AIC and then RW cases, consistent with the results in Figure 4. For lightning in the outer rainbands and the whole TC region, LDs in RI, RW, and AIC cases show no significant differences. In RI and AIC cases (Figures 5a and 5c, respectively), LDs are much larger in the inner core than in the outer rainbands and overall TC region, while the LD in RW cases (Figure 5b) is highest in the outer rainbands. Lightning in the outer rainbands responds to RW of the storm intensity (Figure 5b), with LD decreasing with time after intensity change and falling 60% by 24 h after the rapid weakening. In the RI cases, however (Figure 5a), LD in the outer rainbands does not change significantly with the time of intensity change. This indicates that lightning in the inner core may provide information on TC intensity change, and that lightning in the outer rainbands may give specific information on RW.

During RI and RW (Figures 5a and 5b, respectively), the characteristics of inner core lightning are different. With the approach of RI (−24 h and −12 h), LD in the inner core gradually decreases. During the RI period
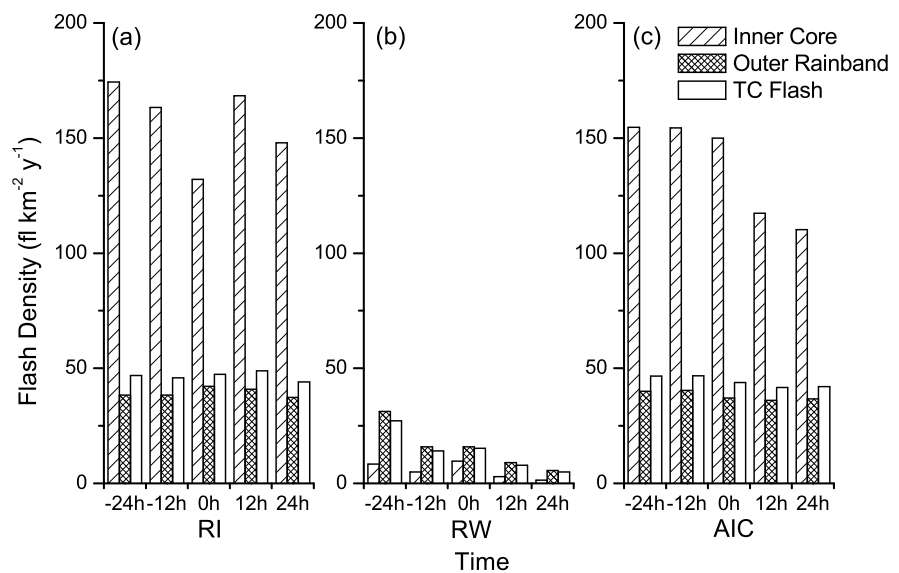
Figure 5. The average LD of the inner core, outer rainbands, and overall TC region as a function of time for RI, RW, and AIC cases. The intensity change occurs at 0 h. The times −24, −12, 12, 24 h refer to 12 h or 24 h before and after intensity change. LD is the average value over the 12 h or 24 h periods before and after the intensity change.
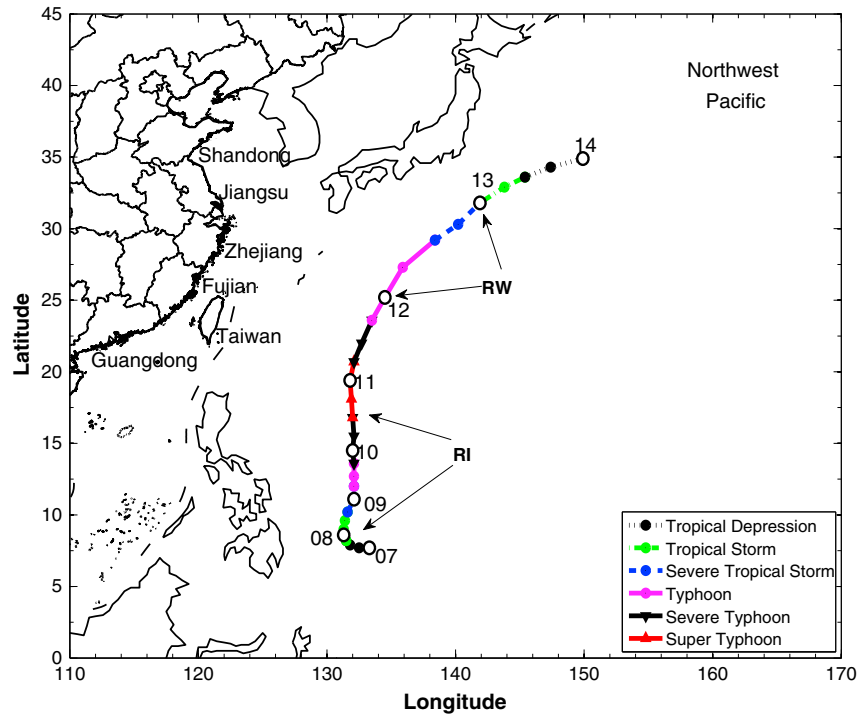
Figure 6. Positions and intensities of Super Typhoon Rammasun. Positions are plotted every 6 h from 0000 UTC 7 May to 0000 UTC 14 May 2008.

(0 h), LD reaches its minimum. After the RI (12 h and 24 h), lightning density begins to increase. In contrast, LD in the inner core first increases with the approach of RW (−24 h and −12 h), reaches its maximum when RW occurs (0 h), and finally decreases after the RW period (12 h and 24 h). Almost no lightning occurs in the inner core at 24 h after the RW. Figure 5b indicates that for RW cases there is a slight increase in inner core lightning when a storm approaches the RW stage.

3.3. Case Study

The statistics above present quantitative results of lightning activity and TC intensity change over the northwest Pacific from observations of a large number of TCs. In this section, an individual case is examined from the perspective of convective structure to study the details that result in different lightning activity. Super Typhoon Rammasun (2008) is selected because it contains all the intensity change categories (RI, AIC, and RW) in its life cycle, so a comparison can be made of convection characteristics in all the different stages in one storm. Additionally, it is one of the most intense storms in the data set and active lightning in the inner core is observed. Hence, the evolution of lightning with intensity change and the reason for lightning outbreaks during RI that emerged from the statistical analyses could be demonstrated.

Rammasun formed from a tropical depression near the Palau Islands in the northwest Pacific. At 1800 UTC 7 May 2008, it evolved into a tropical storm and turned northward. Continuous rapid development followed, and the storm intensified to a strong tropical storm at 1800 UTC 8 May, a typhoon at 0600 UTC 9 May, and a strong typhoon at 1800 UTC 9 May. Rammasun became a super typhoon at 1200 UTC 10 May, 3 days after its formation, with maximum sustained wind of $55 \, \mathrm{m \, s^{-1}}$ and minimum pressure of 935 hPa. It turned north-northeast and weakened into an extratropical cyclone and dissipated over the ocean east of Japan on 14 May 2008. Figure 6 gives the 6 h positions and intensities of Rammasun during its life cycle.

Figure 7 shows the temporal variation of lightning in the inner core and overall TC region plotted together with hourly interpolated maximum sustained wind speed for Super Typhoon Rammasun. Figure 8 gives the distribution of lightning during the development of the TD, RI, and RW stages, overlaid on the minimum TBB. The most frequent lightning occurred at 0300 UTC 7 May with a maximum flash rate of $266 \, \mathrm{fl \, h^{-1}}$ (Figure 7a). The storm had just reached TD intensity at this time, and most lightning appeared
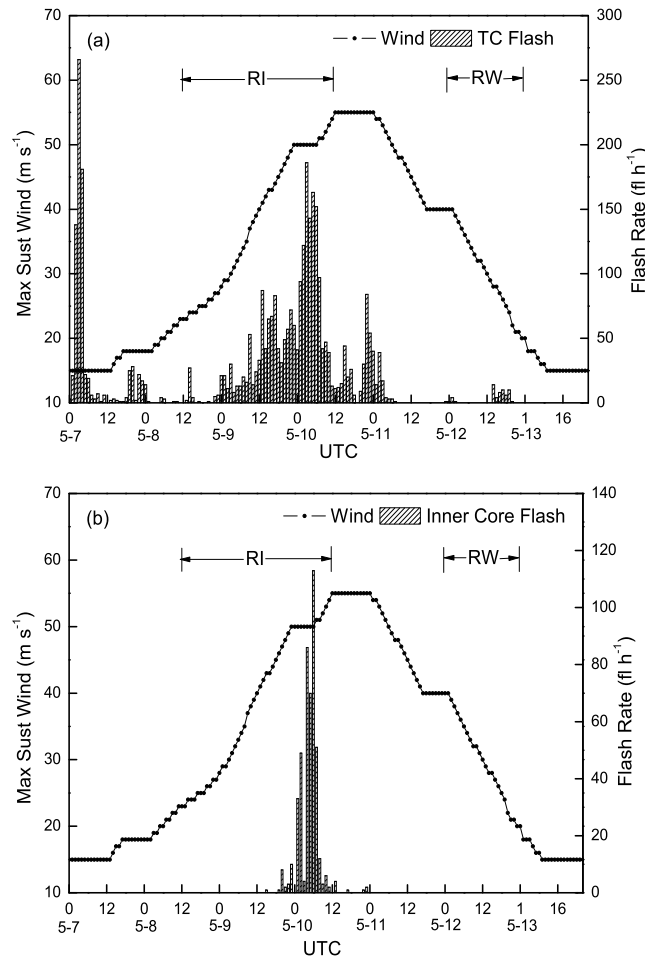
Figure 7. Temporal evolution of lightning flash rate in (a) the overall TC region and (b) the inner core for Super Typhoon Rammasun (2008), superimposed on hourly interpolated maximum sustained wind speed.

200–300 km north of the center in the outer rainbands (Figures 8a and 8b). The TC flash rates decreased dramatically until 1200 UTC 8 May when the storm began to rapidly intensify. The maximum sustained surface winds increased from 23 to $55\,m\,s^{-1}$ over the 48 h RI period, and then the peak wind of $55\,m\,s^{-1}$ was maintained for 12 h (Figure 7a). The TC flash rate increased with the maximum sustained wind speed and reached its secondary peak during the RI stage. High cloud top height and cold cloud top temperature were observed during the RI stage, and active lightning occurred in the inner core region (Figures 8c and 8d). During the RW stage from 0000 UTC 12 May to 0000 UTC 13 May, storm intensity dropped rapidly from 40 to $20\,m\,s^{-1}$ and lightning activity decreased, with only 64 flashes in 24 h. The storm had a loose structure with weak convective activity and high minimum TBB values during the RW period (Figures 8e and 8f).

The most obvious feature of lightning in the inner core for Super Typhoon Rammasun (2008) is that lightning occurred only during the RI stage that began at 1200 UTC 8 May and ended at 1200 UTC 10 May (Figure 7b). Generally, the majority of TC lightning occurred in the outer rainbands of the storm, but the number of inner core lightning flashes increased dramatically during the RI stage and the proportion of lightning in the outer rainbands decreased sharply. The outbreak of inner core lightning during the RI period resulted in a ratio of inner core lightning to TC lightning that reached a maximum of 75%. While Rammasun was at maximum intensity, lightning was observed in the inner core but the flash rates were much smaller than in the RI stage. The fluctuations in Figure 7 show no clear relationship between overall TC lightning and storm intensity for Rammasun. However, the fluctuations represent only lightning in the outer rainbands rather than in the inner core. The inner core lightning gives the most direct information on the RI of Rammasun.

The cumulative distribution functions (CDF) of minimum TBB in the inner core for different intensity change categories are compared in Figure 9. Significant differences in minimum TBB exist in the inner core between RI and the other two intensity change groups. The RI stage has the highest cloud top height and all the minimum TBB values are less than 200 K, compared with only 64% of AIC cases and 9% of RW cases (Table 4). A good relationship is seen between the rate of storm intensification and percentage of cloud tops in the inner core with minimum TBB of 180–240 K (between 0% and 87%), with RI giving the highest cloud top height, followed by AIC and then RW. However, RW cases have more cloud tops at the warmest values (250–280 K, between 87% and 100%) than the AIC cases. Statistical results for minimum TBB and lightning in the inner core region for different intensity change categories show that the range of minimum TBB values is 177.5–288.4 K for RI stages, 180.4–291.8 K for AIC stages, and 199.3–290.5 K for RW stages (Table 4). The mean value of minimum TBB in the inner core is significantly lower for RI cases
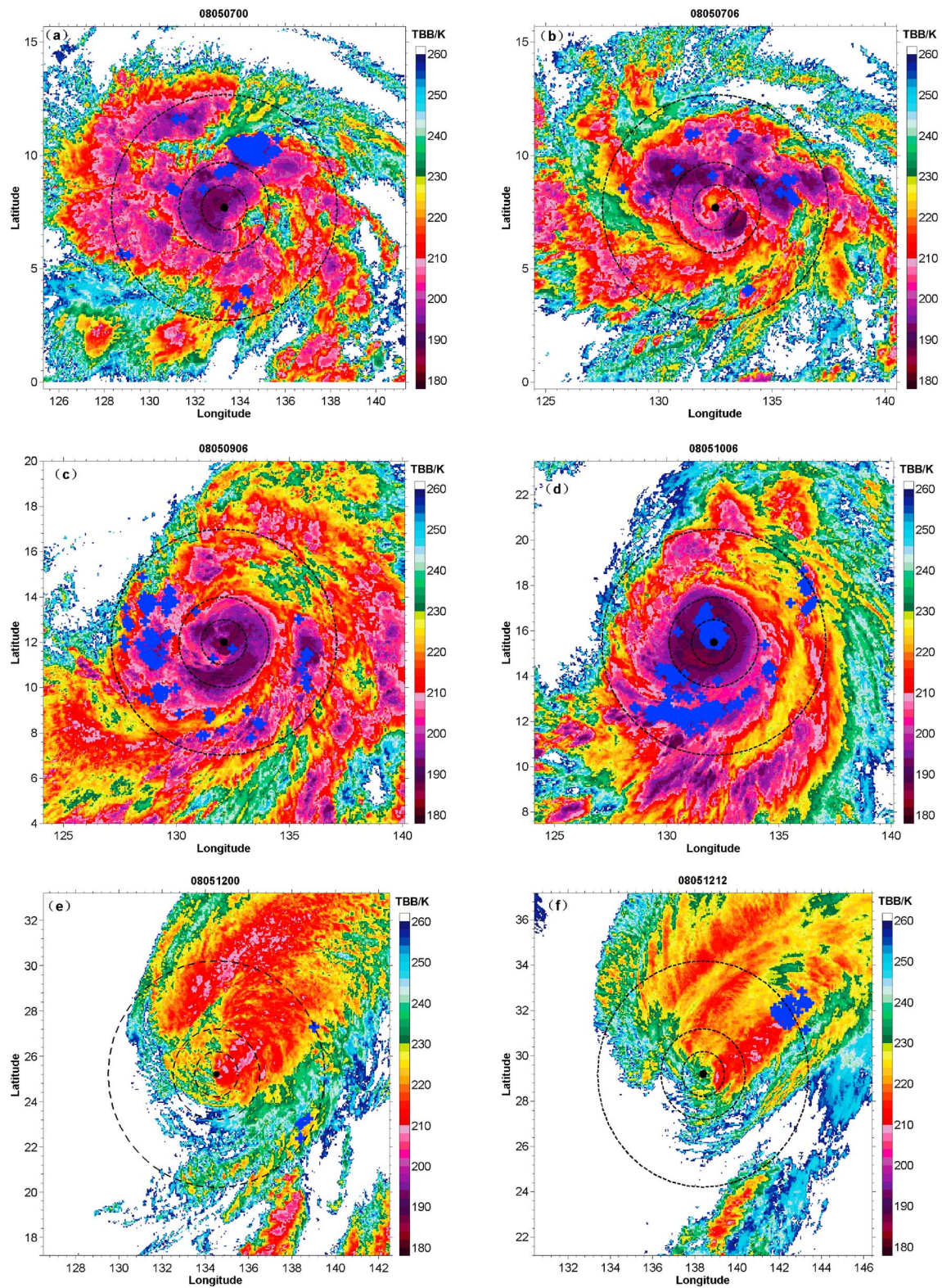
Figure 8. Examples of lightning data overlain on minimum TBB for Rammasun at (a) 0000 UTC 7 May and (b) 0600 UTC 7 May during TD stages; (c) 0600 UTC 9 May and (d) 0600 UTC 10 May during RI stages; and at (e) 0000 UTC 12 May and (f) 1200 UTC 12 May 2008 during RW stages. The central black dot denotes the center location of the storm. The blue crosses in each image indicate lightning detected by WWLLN. The three rings are at ranges of 100, 200, and 500 km. Lightning data are collected 6 h after the observation time. Figures are presented every 6 h, consistent with the best track. The TBB value in each grid cell is the minimum over each 6-hourly period.
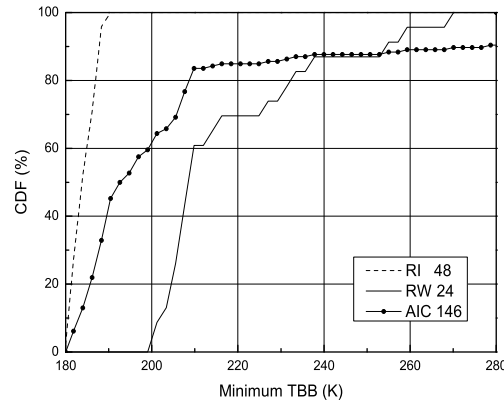
Figure 9. Cumulative distribution function (CDF) of minimum TBB observed by satellite MTSAT-1R in the inner core for Super Typhoon Rammasun (2008) in different intensity change categories: RI, AIC, and RW. The numbers in the figure indicate the sample size for each category.

(199.6 K) than for AIC (225.4 K) and RW (248.3 K). As for lightning rate in the inner core, the value for RI cases (9.5 fl h^{-1}) is about 3 times the value for AIC cases (3.2 fl h^{-1}); no flashes were observed in RW cases.

4. Discussion

4.1. Lightning Patterns in the Pacific Basin

The radial distribution of lightning flash density for the RW, AIC, and RI cases for the northwest Pacific (Figure 4) shows that in the eyewall region, RI cases have the largest LD, followed by AIC, and then RW. There tends to be a different pattern in the relationship between lightning distribution and TC intensity change in the eyewall in the Atlantic, East Pacific, and northwest Pacific basins, for *DeMaria et al.* [2012] found that the largest eyewall LD occurred for RW cases in Atlantic TCs and for AIC cases in East Pacific TCs. This may be caused by the different physical processes occur in Atlantic and Pacific storms [*DeMaria et al.*, 2012]. However, the distributions of LD in the outer rainbands are very similar for all basins, with RI cases possessing the highest LD.

Figure 10 shows the relationship between the vertical wind shear and LD for the inner core and outer rainbands for the northwest Pacific samples used in this study. A two-regime structure relationship (Figure 10a) is apparent for LD in the inner core and the vertical wind shear: LD increases with weak and medium shear and then decreases with strong shear. There is a weak tendency (Figure 10b) for the LD to decrease with increasing wind shear in the outer rainbands. It shows that the relationships between the two variables over the northwest Pacific have the same pattern as those for the Atlantic samples described by *DeMaria et al.* [2012]. This indicates that vertical wind shear does not contribute to the differences in lightning activity between different basins.

DeMaria et al. [2012] discussed the impact of very strong sea surface temperature gradients and found that when the effect of very cold water is removed, the LD distribution for East Pacific storms was similar to that for the Atlantic. Predictors for TC RI change were also found to be different between the Atlantic and Pacific basins [*Kaplan et al.*, 2010], which suggests that the large-scale environmental impact factors are different in different basins. Furthermore, the different pattern of lightning might also be due to atmospheric aerosol differences between the basins. The increased aerosol in the Atlantic may enhance charge generation and thus explain the higher LD observed for Atlantic than for East Pacific cyclones [*Sherwood*, 2002; *Khain et al.*, 2008]. Therefore, the relationship between lightning activity and storm intensity in one basin may not be applicable in another, and it is important to investigate individual relationships between electrical organization and convective structure.

4.2. Implications of Inner Core Lightning for Rapid Intensity Change

The possibility of using lightning data to forecast rapid intensity change of TCs has been investigated in many studies [*Lyons et al.*, 1989; *Molinari et al.*, 1994, 1999; *Samsury and Orville*, 1994; *Shao et al.*, 2005; *Squires and Businger*, 2008; *Zhang et al.*, 2012]. With the same data set as used in this study, *Pan et al.* [2014] found the

Table 4. Statistics for Minimum TBB and Lightning in the Inner Core of Rammasun (2008) for Different Intensity Change Categories

Intensity Change	Hours	TBB (K)				TBB Pixel Counts (%)			Flash Count		Flash Rate (fl h^{-1})	
		Minimum	Maximum	Mean	SD	≤190 K	≤200 K	≤220 K	TC	Inner Core	TC	Inner Core
RI	48	177.5	288.4	199.6	14.3	100	100	100	2117	454	44.1	9.5
AIC	146	180.4	291.8	225.4	33.3	45	64	85	2856	461	19.6	3.2
RW	24	199.3	290.5	248.3	27.1	0	9	70	59	0	2.5	0
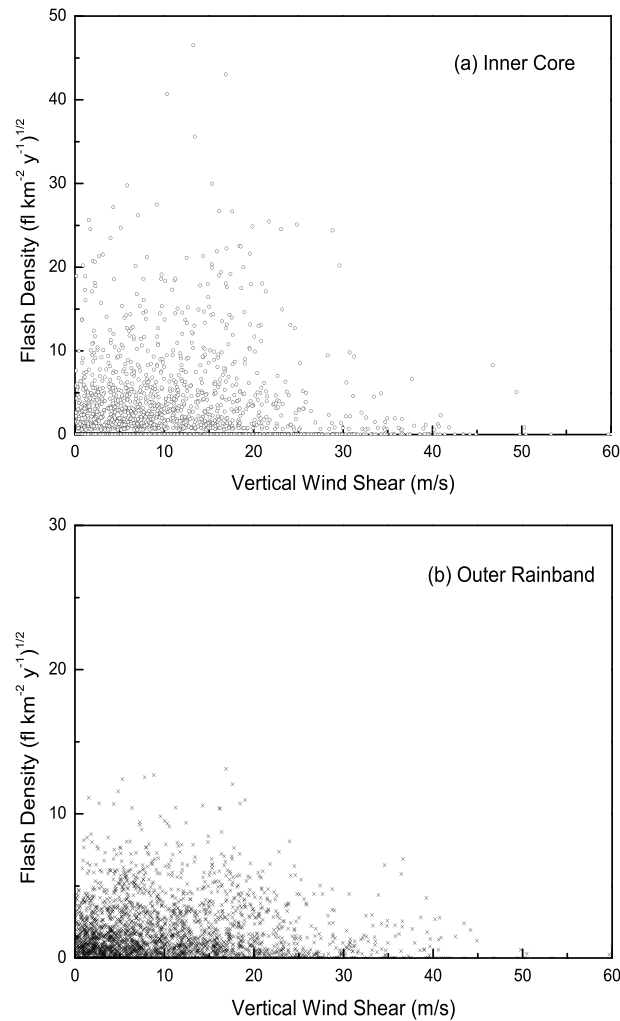
Figure 10. Scatterplots of the vertical wind shear against the square root of lightning density for (a) the inner core and (b) the outer rainband.

average LD in the inner core of super (Categories 4–5) typhoons was more than twice that for weak (Categories 1–3) typhoons. Our study confirms the results from previous studies: the average LD is largest in the inner core of all the regions of storms, with tropical storms have more lightning than typhoons and super typhoons, and LD in intensifying storms is greater than in weakening storms. The results of this study also provide additional evidence that lightning activity in the inner core may be a better indicator than lightning activity in outer rainbands for the prediction of intensity change of TCs in the northwest Pacific.

TC intensity change is forced by large-scale environment factors such as vertical wind shear, sea surface temperature, and warm ocean eddy interactions. However, the importance of inner core processes for TC intensity change has also been examined by many researchers. *Willoughby et al.* [1982] suggested that significant increases in TC intensity occurred when an outer eyewall contracted and replaced the inner eyewall, and *Sitkowski and Barnes* [2009] reported a "spiraling in" of the eyewall initiated the RI of Hurricane Guillermo (1997). Theoretical and modeling results [e.g., *Kossin and Schubert*, 2001] also show that favorable localized positive mesovortices within the inner core may lead to TC intensification. Changes in lightning patterns in the inner core region reflect changes in the convective structure of the storm, and an outbreak of inner core lightning reflects strong mesoscale convection that leads in turn to RI. The U.S. Weather Research Program has been trying to assimilate lightning data into models to predict the path and intensity of hurricanes [*Marks and Shay*, 1998]. Some recent studies have also tested and proven the forecasting ability of lightning data in the Statistical Hurricane Intensity Prediction Scheme model [*DeMaria*, 1996, *DeMaria et al.*, 2012] and other numerical models [*Fierro et al.*, 2007; *Fierro and Reisner*, 2011]. *DeMaria et al.* [2012] pointed out that the relationship between lightning and other physical variables is strongly nonlinear, so the assimilation of lightning data into atmospheric models is a challenging problem. Issues associated with the physical mechanisms relating lightning activity to TC intensity change require further study.

5. Conclusions

Lightning data from the WWLLN along with TC track and intensity data from the China Meteorological Administration best-track data set were used to study lightning activity in TCs over the northwest Pacific from 2005 to 2009 and to investigate the relationship between inner core lightning and TC intensity changes. Lightning was analyzed for storms undergoing three categories of intensity change: RI, AIC, and RW. A case study of Super Typhoon Rammasun (2008) was also examined to study the results from statistical analyses and gave details for lightning activity from the perspective of convective structure. The main results of this study are summarized as follows.

Lightning is more likely to occur in storms at TD and TS intensity levels; these two groups contain the largest number of observed ITPs including lightning. There is a gradual decrease in ITP number as the intensity level of the storm increases. Changes in flash density with TC intensity level show the same trend in the inner core and outer rainbands, with first an increase in weak storms (TD and TS) and then a decrease in storms stronger than STS. Lightning occurs most often in TS intensity storms in the inner core and least in STY intensity storms. For the outer rainbands, lightning also occurs most frequently in TS intensity, but the minimum flash density appears in storms at SuperTY intensity.

Rapid intensity changes (RI and RW) represent a very small proportion (8% and 1%, respectively) of intensity change cases, and storms are generally in a relatively stable state (AIC, 91%) when over water. Obvious differences in the geographical distribution of RI and RW cases including lightning are shown. RI generally occurs at low latitudes south of 25°N and north of 5°N, while RW cases tend to occur at higher latitudes, from 20° to 40°N, east of 125°E. Lightning is observed in both RI and RW cases. Lightning in RI cases is most likely to occur in TS intensity storms, and there are no RI cases including lightning when the storm reaches SuperTY intensity. In contrast to RI, all RW cases including lightning are from TCs at typhoon and higher intensity, and no RW cases are from weak storms (TD, TS, or STS).

Lightning occurs more often in storms that strengthen during the next 24 h than in those that weaken. The largest LD in the inner core appears in storms undergoing intensity changes in the range $25 \, \text{m s}^{-1} > \Delta V_{\text{max24}} \geq 15 \, \text{m s}^{-1}$ (i.e., RI) during the next 24 h. The LD for RI cases is larger than for RW cases in all radial bins, especially in the inner core region (0–100 km), with LD about 4.2 times greater for RI cases than for RW cases. The differences in LD between RI and RW reach a maximum in the inner core but there are no significant differences in the outer rainbands. The LD in RW cases is higher in the outer rainbands than in the inner core and overall TC region. This result suggests that lightning activity in the inner core has predictive information for the RI of storms, and lightning in the outer rainbands may give information on RW.

The amount of inner core lightning for Super Typhoon Rammasun (2008) increased dramatically during the RI stage, and the proportion of lightning in the outer rainbands decreased sharply. The outbreak of inner core lightning during the RI period resulted in the ratio of the inner core lightning to TC lightning reaching a maximum of 75%. Observations of convective structure from satellite data showed that the RI stage had the highest cloud top height and coldest cloud top temperature; all the minimum TBB values at the RI stage were below 200 K. The mean value of minimum TBB in the inner core was significantly lower for RI (199.6 K) than for AIC (225.4 K) and RW (248.3 K). During RW periods, the storm had a loose structure with weak convective activity and high minimum TBB values. These significant differences in convective characteristics among different intensity change categories in the inner core help reveal why lightning outbreaks occur during the RI of the storm.

References

Abarca, S. F., K. L. Corbosiero, and T. J. Galarneau Jr. (2010), An evaluation of the Worldwide Lightning Location Network (WWLLN) using the National Lightning Detection Network (NLDN) as ground truth, *J. Geophys. Res.*, 115, D18206, doi:10.1029/2009JD013411.

Abarca, S. F., K. L. Corbosiero, and D. Vollaro (2011), The World Wide Lightning Location Network and convective activity in tropical cyclones, *Mon. Weather Rev.*, 139, 175–191.

Abreu, D., D. Chandan, R. H. Holzworth, and K. Strong (2010), A performance assessment of the World Wide Lightning Location Network (WWLLN) via comparison with the Canadian Lightning Detection Network (CLDN), *Atmos. Meas. Tech.*, 3(4), 1143–1153.

Black, R. A., and J. Hallett (1986), Observations of the distribution of ice in hurricanes, *J. Atmos. Sci.*, 43, 802–822.

Black, R. A., and J. Hallett (1999), Electrification of the hurricane, *J. Atmos. Sci.*, 56, 2004–2028.

Black, M. L., R. W. Burpee, and F. D. Marks Jr. (1996), Vertical motion characteristics of tropical cyclones determined with airborne Doppler radial velocities, *J. Atmos. Sci.*, 53, 1887–1909.

Boccippio, D. J., W. J. Koshak, and R. J. Blakeslee (2002), Performance assessment of the optical transient detector and lightning imaging sensor. Part I: Predicted diurnal variability, *J. Atmos. Oceanic Technol.*, 19, 1318–1332.

Bovalo, C., C. Barthe, and N. Bègue (2012), A lightning climatology of the South-West Indian Ocean, *Nat. Hazards Earth Syst. Sci.*, 12, 2659–2670.

Bovalo, C., C. Barthe, N. Yu, and N. Bègue (2014), Lightning activity within tropical cyclones in the South West Indian Ocean, *J. Geophys. Res. Atmos.*, 119, 8231–8244, doi:10.1002/2014JD021651.

Brand, S. (1973), Rapid intensification and low-latitude weakening of tropical cyclones of the western North Pacific Ocean, *J. Appl. Meteorol.*, 12, 94–103.

Cecil, D. J., and E. J. Zipser (1999), Relationships between tropical cyclone intensity and satellite-based indicators of inner core convection: 85-GHz ice-scattering signature and lightning, *Mon. Weather Rev.*, 127, 103–123.

Cecil, D. J., D. E. Buechler, and R. J. Blakeslee (2014), Gridded lightning climatology from TRMM-LIS and OTD: Dataset description, *Atmos. Res.*, 135–136, 404–414.

DeMaria, M. (1996), The effect of vertical shear on tropical cyclone intensity change, *J. Atmos. Sci., 53*, 2076–2087.

DeMaria, M., and R. T. DeMaria (2009), Applications of lightning observations to tropical cyclone intensity forecasting, paper presented at 16th Conference on Satellite Meteorology and Oceanography, Am. Meteorol. Soc., Phoenix, Ariz. [Available at http://ams.confex.com/ams/89annual/techprogram/paper_145745.htm.]

DeMaria, M., R. T. DeMaria, J. A. Knaff, and D. Molenar (2012), Tropical cyclone lightning and rapid intensity change, *Mon. Weather Rev., 140*, 1828–1842.

DeMaria, M., C. R. Sampson, J. A. Knaff, and K. D. Musgrave (2014), Is tropical cyclone intensity guidance improving?, *Bull. Am. Meteorol. Soc., 95*, 387–398.

Demetriades, N. W. S., M. J. Murphy, and J. A. Cramer (2010), Validation of Vaisala's Global Lightning Dataset (GLD360) over the continental United States, paper presented at 29th Conf. Hurricanes and Tropical Meteorology, Am. Meteorol. Soc., Tucson, Ariz., 10–14 May.

Dowden, R. L., J. B. Brundell, and C. J. Rodger (2002), VLF lightning location by time of group arrival (TOGA) at multiple sites, *J. Atmos. Sol. Terr. Phys., 64*, 817–830.

Fierro, A. O., and J. M. Reisner (2011), High-resolution simulation of the electrification and lightning of Hurricane Rita during the period of rapid intensification, *J. Atmos. Sci., 68*, 477–494.

Fierro, A. O., L. Leslie, E. Mansell, J. Straka, D. MacGorman, and C. Ziegler (2007), A high-resolution simulation of microphysics and electrification in an idealized hurricane-like vortex, *Meteorol. Atmos. Phys., 98*, 13–33.

Fierro, A. O., X. M. Shao, T. Hamlin, J. M. Reisner, and J. Harlin (2011), Evolution of eyewall convective events as indicated by intracloud and cloud-to-ground lightning activity during the rapid intensification of hurricanes Rita and Katrina, *Mon. Weather Rev., 139*, 1492–1504.

Hutchins, M. L., R. H. Holzworth, J. B. Brundell, and C. J. Rodger (2012), Relative detection efficiency of the World Wide Lightning Location Network, *Radio Sci., 47*, RS6005, doi:10.1029/2012RS005049.

Jacobson, A. R., R. H. Holzworth, J. Harlin, R. L. Dowden, and E. H. Lay (2006), Performance assessment of the World Wide Lightning Location Network (WWLLN), using the Los Alamos Sferic Array (LASA) as ground truth, *J. Atmos. Oceanic Technol., 23*, 1082–1092.

Jiang, H. (2012), The relationship between tropical cyclone intensity change and the strength of inner-core convection, *Mon. Weather Rev., 140*, 1164–1176.

Jiang, H., E. M. Ramirez, and D. J. Cecil (2013), Convective and rainfall properties of tropical cyclone inner cores and rainbands from 11 years of TRMM data, *Mon. Weather Rev., 141*, 431–450.

Kaplan, J., and M. DeMaria (2003), Large-scale characteristics of rapidly intensifying tropical cyclones in the North Atlantic basin, *Weather Forecasting, 18*, 1093–1108.

Kaplan, J., M. DeMaria, and J. A. Knaff (2010), A revised tropical cyclone rapid intensification index for the Atlantic and eastern North Pacific basins, *Weather Forecasting, 25*, 220–241.

Kelley, O. A., J. Stout, and J. B. Halverson (2004), Tall precipitation cells in tropical cyclone eyewalls are associated with tropical cyclone intensification, *Geophys. Res. Lett., 31*, L24112, doi:10.1029/2004GL021616.

Kelley, O. A., J. Stout, and J. B. Halverson (2005), Hurricane intensification detected by continuously monitoring tall precipitation in the eyewall, *Geophys. Res. Lett., 32*, L20819, doi:10.1029/2005GL023583.

Khain, A., N. Cohen, B. Lynn, and A. Pokrovsky (2008), Possible aerosol effects on lightning activity and structure of hurricanes, *J. Atmos. Sci., 65*, 3652–3677.

Kossin, J., and W. H. Schubert (2001), Mesovortices, polygonal flow patterns, and rapid pressure falls in hurricane-like vortices, *J. Atmos. Sci., 58*, 2196–2209.

Lay, E. H., R. H. Holzworth, C. J. Rodger, J. N. Thomas, O. Pinto Jr., and R. L. Dowden (2004), WWLL global lightning detection system: Regional validation study in Brazil, *Geophys. Res. Lett., 31*, L03102, doi:10.1029/2003GL018882.

Liu, K. S., and J. C. L. Chan (1999), Size of tropical cyclones as inferred from ERS-1 and ERS-2 data, *Mon. Weather Rev., 127*, 2992–3001.

Lyons, W. A., and C. S. Keen (1994), Observations of lightning in convective supercells within tropical storms and hurricanes, *Mon. Weather Rev., 122*(8), 1897–1916.

Lyons, W. A., M. G. Venne, P. G. Black, and R. C. Gentry (1989), Hurricane lightning: A new diagnostic tool for tropical storm forecasting? Preprints, 18th Conf. on Hurricanes and Tropical Meteorology, 113–11, Am. Meteorol. Soc., San Diego, Calif.

MacGorman, D. R., and C. D. Morgenstern (1998), Some characteristics of cloud-to-ground lightning in mesoscale convective systems, *J. Geophys. Res., 103*, 14,011–14,023, doi:10.1029/97JD03221.

Marks, F. D., and L. K. Shay (1998), Landfalling tropical cyclones: Forecast problems and associated research opportunities, *Bull. Am. Meteorol. Soc., 79*(2), 305–323.

Merrill, R. T. (1984), A comparison of large and small tropical cyclones, *Mon. Weather Rev., 112*, 1408–1418.

Molinari, J., P. K. Moore, V. P. Idone, R. W. Henderson, and A. B. Saljoughy (1994), Cloud-to-ground lightning in Hurricane Andrew, *J. Geophys. Res., 99*(D8), 16,665–16,676, doi:10.1029/94JD00722.

Molinari, J., P. Moore, and V. Idone (1999), Convective structure of hurricanes as revealed by lightning locations, *Mon. Weather Rev., 127*, 520–534.

Nolan, D. S., Y. Moon, and D. P. Stern (2007), Tropical cyclone intensification from asymmetric convection: Energetics and efficiency, *J. Atmos. Sci., 64*, 3377–3405.

Pan, L., X. Qie, D. Liu, D. Wang, and J. Yang (2010), The lightning activities in super typhoons over the Northwest Pacific, *Sci. China, Ser. D: Earth Sci., 53*(8), 1241–1248.

Pan, L., D. Liu, X. Qie, D. Wang, and R. Zhu (2013), Land-sea contrast in the lightning diurnal variation as observed by the WWLLN and LIS/OTD Data, *Acta Meteorol. Sin., 27*(4), 591–600.

Pan, L., X. Qie, and D. Wang (2014), Lightning activity and its relation to the intensity of typhoons over the Northwest Pacific Ocean, *Adv. Atmos. Sci., 31*(3), 581–592.

Price, C., M. Asfur, and Y. Yair (2009), Maximum hurricane intensity preceded by increase in lightning frequency, *Nat. Geosci., 2*, 329–332.

Reinhart, B., H. Fuelberg, R. Blakeslee, D. Mach, A. Heymsfield, A. Bansemer, S. L. Durden, S. Tanelli, G. Heymsfield, and B. Lambrigtsen (2014), Understanding the relationships between lightning, cloud microphysics, and airborne radar-derived storm structure during Hurricane Karl (2010), *Mon. Weather Rev., 142*, 590–605.

Rodger, C. J., J. B. Brundell, R. L. Dowden, and N. R. Thomson (2004), Location accuracy of long distance VLF lightning location network, *Ann. Geophys., 22*, 747–758.

Rodger, C. J., J. B. Brundell, and R. L. Dowden (2005), Location accuracy of VLF World-Wide Lightning Location (WWLL) network: Post-algorithm upgrade, *Ann. Geophys., 23*(2), 277–290.

Rodger, C. J., S. Werner, J. B. Brundell, E. H. Lay, N. R. Thomson, R. H. Holzworth, and R. L. Dowden (2006), Detection efficiency of the VLF World-Wide Lightning Location Network (WWLLN): Initial case study, *Ann. Geophys., 24*, 3197–3214.

Rodger, C. J., J. B. Brundell, R. H. Holzworth, and E. H. Lay (2008), Growing detection efficiency of the World Wide Lightning Location Network, *Coupling of Thunderstorms and Lightning Discharges to Near-Earth Space: Proceedings of the Workshop, AIP Conference Proceedings*, vol. 1118, pp. 15–20, doi:10.1063/1.3137706, 23–27 June.

Rust, W. D., W. L. Taylor, D. R. MacGorman, and R. T. Arnold (1981), Research on electrical properties of severe thunderstorms in the Great Plains, *Bull. Am. Meteorol. Soc.*, *62*, 1286–1293.

Rutledge, S. A., E. R. Williams, and W. A. Petersen (1993), Lightning and electrical structure of mesoscale convective systems, *Atmos. Res.*, *29*, 27–53.

Samsury, C. E., and R. E. Orville (1994), Cloud-to-ground lightning in tropical cyclones: A study of Hurricanes Hugo (1989) and Jerry (1989), *Mon. Weather Rev.*, *122*(8), 1887–1896.

Shao, X.-M., J. Harlin, M. Stock, M. Stanley, A. Regan, K. Wiens, T. Hamlin, M. Pongratz, D. Suszcynsky, and T. Light (2005), Katrina and Rita were lit up with lightning, *Eos Trans. AGU*, *86*(42), 398–398, doi:10.1029/2005EO420004.

Shen, B.-W., R. Atlas, O. Reale, S.-J. Lin, J.-D. Chern, J. Chang, C. Henze, and J.-L. Li (2006), Hurricane forecasts with a global mesoscale-resolving model: Preliminary results with Hurricane Katrina (2005), *Geophys. Res. Lett.*, *33*, L13813, doi:10.1029/2006GL026143.

Sherwood, S. C. (2002), Aerosols and ice particle size in tropical cumulonimbus, *J. Clim.*, *15*, 1051–1063.

Shu, S. J., J. Ming, and P. Chi (2012), Large-scale characteristics and probability of rapidly intensifying tropical cyclones in the western North Pacific basin, *Weather Forecasting*, *27*, 411–423.

Sitkowski, M., and G. M. Barnes (2009), Low-level thermodynamic, kinematic, and reflectivity fields of Hurricane Guillermo (1997) during rapid intensification, *Mon. Weather Rev.*, *137*, 645–663.

Solorzano, N. N., J. N. Thomas, and R. H. Holzworth (2008), Global studies of tropical cyclones using the World Wide Lightning Location Network, Preprints, third conference on the Meteorological Applications of Lightning Data, Am. Meteorol. Soc., New Orleans, La., 1.4.

Squires, K., and S. Businger (2008), The morphology of eyewall lightning outbreaks in two category 5 hurricanes, *Mon. Weather Rev.*, *136*, 1706–1726.

Taniguchi, K., and T. Koike (2008), Seasonal variation of cloud activity and atmospheric profiles over the eastern part of the Tibetan Plateau, *J. Geophys. Res.*, *113*, D10104, doi:10.1029/2007JD009321.

Thomas, J. N., N. N. Solorzano, S. A. Cummer, and R. H. Holzworth (2010), Polarity and energetics of inner core lightning in three intense North Atlantic hurricanes, *J. Geophys. Res.*, *115*, A00E15, doi:10.1029/2009JA014777.

Virts, K. S., J. M. Wallace, M. L. Hutchins, and R. H. Holzworth (2013), Highlights of a new ground-based, hourly global lightning climatology, *Bull. Am. Meteorol. Soc.*, *94*, 1381–1391.

Willoughby, H. E., J. A. Clos, and M. G. Shoreibah (1982), Concentric eye walls, secondary wind maxima, and the evolution of the hurricane vortex, *J. Atmos. Sci.*, *39*, 395–411.

Zhang, W., Y. Zhang, D. Zheng, and X. Zhou (2012), Lightning distribution and eyewall outbreaks in tropical cyclones during landfall, *Mon. Weather Rev.*, *140*, 3573–3586.

Zhang, W., Y. Zhang, and X. Zhou (2013), Lightning activity and precipitation characteristics of Typhoon Molave (2009) around its landfall, *Acta Meteorol. Sin.*, *27*(5), 742–757.